Numerical investigation of cycle performance in compressed air energy storage in aquifers

Lichao Yang[a], Zuansi Cai[b], Cai Li[c], Qingcheng He[d], Yan Ma[d], Chaobin Guo [d,*]

[a] School of Water Resources and Environment, China University of Geosciences (Beijing), Beijing 100083, China
[b] School of Engineering and the Built Environment, Edinburgh Napier University, Edinburgh EH10 5DT, UK
[c] School of Civil Engineering, the University of Sydney, NSW 2006, Australia
[d] Chinese Academy of Geological Sciences, Beijing 100037, China

Abstract: Compressed air energy storage (CAES) is one of the promising technologies to store the renewable energies such as surplus solar and wind energy in a grid scale. Due to the widespread of aquifers in the world, the compressed air energy storage in aquifers (CAESA) has advantages compared with the compressed air energy storage in caverns and air tanks. The feasibility of aquifers as storage media in CAES system has been demonstrated by numerical models and field tests. This study proposes a numerical model by Transport of Unsaturated Groundwater and Heat Version 3.0/Equation-of-State 3 (TOUGH3/EOS3) to simulate a field-scale study of a novel CAES by storing the compressed air in aquifers. The feasibility of the model has been demonstrated by comparison of simulation results and monitoring data. After that, three types of cycles, which are daily cycle, weekly cycle and monthly cycle, are designed to study their performance within a month working cycle. Their gas saturation show small differences after one month cycle. When the air with temperature of 50°C injected into aquifers with temperature of 20°C, after the cycle finished, the air temperature in aquifer of daily cycle are 5.4°C higher than that of weekly cycle and 10.8°C higher than that of monthly cycle. It is indicated that during the same cycle periods, the more cycle times, the higher air temperature in aquifers after the cycle. The energy recovery efficiencies for daily cycle, weekly cycle and monthly cycle are 96.96%, 96.27% and 93.15%, respectively. The slight increase of energy recovery efficiencies from daily cycle to monthly cycle indicate that with the same energy storage scales, the energy produced by daily cycle has slight competitiveness. The simulation results can provide references for engineering application in future.

Keywords: aquifers**;** compressed air energy storage; numerical model; cycles; energy recovery efficiency

1. Introduction

Renewable energies hold a lot of promise when it comes to replace the conventional energy sources such as fossil fuels and coal. The intermittence of them, however, will greatly constrain the utilization efficiency. Therefore, the grid-scale energy storage technologies are required to improve the stability and utilization rate of the renewable energies. To date, the largest sources of grid-scale electrical energy storage today are pumped hydro storage (PHS) at 127 GW and compressed air energy storage (CAES) at 400 MW [1]. Research on PHS, especially on cascade reservoirs joint operation research has been conducted in recent years [2,3]. Among other energy storage technologies (e.g., battery and flywheel energy storage), CAES has been demonstrated as a promising technology for its large storage scale, economic feasibility, high reliability and low environmental influence [4,5]. The basic principles, past milestones and recent development (1975-2015) of CAES have been reviewed in detail by Budt M et al. Moreover, a comprehensive classification and comparison of different CAES technologies as well as some challenging issues about CAES research and development have been addressed [6]. The geological resource potential of the CAES technology worldwide by overlying suitable geological formations, salt deposits and aquifers was presented by Aghahosseini A et al. The geological resource potential for the world was divided into 145 regions, in which the potential of CAES in each region was assessed and a relevant map was provided [7].

[*] Corresponding author: Chaobin Guo, Email address: guochaobin123@hotmail.com

The feasibility and requirements of CAES have been proved by energy storage in air tanks, underground caverns and aquifers [8]. Air tank is considered as micro-CAES to conduct research with relatively small storage scale [9,10]. In terms of grid scale CAES system, the feasibility and application has been demonstrated by compressed air energy storage in caverns in many studies [6,8]. The only two commercial grid-scale CAES facilities operated in the world use underground carven as storage media [11.12]. One facility is in Huntorf, Germany (290MW) and the other one is in McIntosh, USA (110MW), with a storage efficiency of around 50% [13]. Aquifers has been proved its feasibility as a storage media for compressed air energy storage by field tests [14], mathematical models [15,16] and numerical simulations [4,17,18]. Comparison research of compressed air energy storage in aquifers and caverns further demonstrated the feasibility of CAESA and its performance can be similar to or better than compressed air energy storage in caverns [19]. The advantage of CAESA against the conventional CAES is of wide availability as well as lower economic costs [20]. The feasibility of cyclical air injection and withdrawal at ambient and elevated temperatures in an aquifer reservoir was demonstrated by a CAESA field test in Pittsfield, USA [21,22].

Many factors can affect the performance of CAESA system. A 1D numerical model to investigate the cycling of flow field by heating day air injection around a single well in an aquifer provided the primary understanding about the performance of an aquifer for CAES [23]. This research stated that permeability and mass flow rate per unit thickness of the aquifer are the major influential factors on hydrodynamic response of the reservoir, and deliverability of compressed air during production will decrease if the air is injected with high temperature. It's shown that there is an optimum permeability range for a candidate aquifer for a certain scale of CAESA system [24]. The increased permeability also leads to increased thermal and exergy efficiencies as well as the increased net output of the CAESA plant [25]. Li Y et al. created the low-permeability barrier in high-permeability aquifers by injecting grout with certain properties using TOUGH2/Gel. The sensitivity studies showed that in a horizontal aquifer, low critical solidification concentrations and small scale factors are generally preferred [26]. Research on aquifer structure of CAESA concluded that the aquifer with anticline structure has a better performance and higher efficiency for CAESA system than syncline and horizontal structure [27,28]. Wiles and Oster found that the near-wellbore area can be fast dehydrated during the bubble development, and the dehydration rates of reservoir increase with increase of injection temperature [29]. Research on utilization of CO_2 as cushion gas for porous media compressed air energy storage indicated that CO_2 cushion gas should be located at the far outer margins of storage reservoirs to avoid air-CO_2 mixing and subsequent production of CO_2 up the well [30]. The impact of injection rate, overall heat transfer coefficient and thermal diffusivity of the formation on heat loss in the wellbore of CAES was analyzed with a semi-analytical solution. It is indicated that a low overall heat transfer coefficient and thermal diffusivity of the formation with an appropriate injection rate can efficiently reduce the heat loss [31]. A hybrid energy storage system using compressed air and hydrogen as the energy carrier is demonstrated that this technology is competitive with pure hydrogen energy storage technology [32]. The economic study on CAES system showed that the investment in adiabatic CAES used for load-leveling purposes was the most economical option [33]. Simulation operation suggested that water coning should not be a severe problem due to the slow response of water to the pressure gradients [21,34]. The oxygen depletion from the stored air caused by chemical reaction, and is believed to be a long-term effect and is not likely to have significant impact in the near-wellbore cycling region [13,35].

How to improve the efficiency of CAES system is one of the key issues during the CAES research. The cycle efficiency of CAES can be described by different equations [36]. The first public experiment on CAES system with thermal energy storage (TES) demonstrated that TES is an effective method to improve the efficiency of CAES and obtain better economy [37,38]. The higher injection air temperature in aquifers has a higher energy storage capability in CAESA system [39]. A novel high temperature hybrid compressed air energy storage (HTH-CAES) system is proved to be more efficient and energy dense compared with an advanced adiabatic design of the same power output [40]. The comparison between a conventional CAES (C-CAES) and a steam-injected CAES (SI-CAES) indicated that steam injection is an effective method for augmenting the power generation of CAES for peak load management [41]. The numerical studies of wellbore flow on CAESA system indicated that a fully penetrating wellbore in CAESA system can obtain better energy efficiencies [42]. A solution using Phase Change

Material (PCM) was carried out to store the heat generated during compression stage for enhancing the efficiency of CAES system. Both theoretical simulation and experimental measurements showed that the use of PCM can effectively reduce the air temperature during charging [43]. The technical and economic research on Adiabatic Compressed Air Energy Storage (A-CAES) and C-CAES showed that the overall efficiency of A-CAES system was better than that of C-CAES system, but the breakeven electricity selling price (BESP) of the A-CAES system was much higher than that of C-CAES system [17]. In order to improve CAES system efficiency, a novel variable pressure ratio CAES system was developed by controlling the opening or closing of valves between compressors and the opening or closing of valves between turbines. It was indicated that this system can not only significantly improve the energy storage efficiency, but also be easy to realize [44]. A conventional exergy analysis was conducted for the grid connected underwater compressed air energy storage facility. It is indicated that the exergy were enhanced by splitting exergy destruction rates into avoidable and unavoidable, as well as endogenous and exogenous parts via advanced exergy analysis [18].

Many research results have been achieved in terms of the investigation of CAES system integrated with renewable energy sources (e.g., wind power and solar power) to overcome the intermittency problem of renewable energies. There are still many challenges in improving the utilization rate of renewable energies with CAES technologies. Besides of Pittsfield test and Huntorf project, many researches on working cycle of CAESA system and efficiency studies are based on short-time cycle. However, the investigation on different cycle modes and their performance to CAESA system are still limited. The intermittent and unstable nature of renewable energies such as wind energy and solar energy imply that they can only be stored at specific periods or even specific seasons. In addition, the various demands of users may signify that peak demand of electricity would be happened in specific periods. Therefore, it is necessary to conduct research on different cycle modes of CAESA system to achieve the maximum utilization rate of renewable energies and meet various demands of users.

This research focuses on two aspects: (1) Is it possible to conduct the different cycle modes in CAESA system? (2) How does the cycle mode affect the performance and energy recovery efficiency of CAESA system? To address these key scientific questions, a 3-D numerical model using TOUGH3/EOS3, based on Pittsfield aquifer field test, were developed to analysis the performance of CAESA system under different working cycle modes, including pressure, gas saturation and temperature. In addition, the energy recovery efficiencies of different designed cycles were analyzed. The conclusions and suggestions were given to provide references for engineering application.

2. Model setup

2.1. Conceptual model

An aquifer field experiment near Pittsfield, Illinois, USA, sponsored by Department of Energy (DOE)/Electric Power Research Institute (EPRI), was carried out in Pike County in 1981 [36,45,46]. Pre-test analysis was carried out to examine the aquifer characterization in four aspects, which were bubble development, water coning, thermal development and near-wellbore desaturation [47,34]. The aquifer parameters were presented by field experiments and indoor experiments [22,48]. This dome-shape site was selected from eleven candidate sites after seismic reflection surveying, drilling, permeability and threshold pressure testing of reservoir and cap rock cores, and hydrostatic head measurement [14]. Early investigation showed that the doubly plunging anticline extends about 25 km with two second-order closures potentially suitable for CAES (Figure 1 (a)). The permeable St. Peter sandstone is beneath the impervious Galena-Platteville-Joachim carbonate cap rock complex. The core tests showed that the cap rock formations are sufficiently impervious to hold the compressed air during the lifetime of the field test [36]. The reservoir is the highly permeable quartz-dominated St. Peter sandstone with a thickness of 69 m. It is composed of three sub-layers, which are green layer (3 m), white layer (6 m) and grey layer (60 m), respectively. The closure closer to Pittsfield (the red box in Figure 1 (a)) was confirmed by a subsequent seismic survey and exploratory drilling with a diameter of 300 m and a closure of 7 to 11 m (Figure 1 (c)), but the other closure was not well defined by the seismic survey [36]. Therefore, the well-depicted closure was used for the compressed air energy storage test. The injection/withdrawal (I/W)

well was located at the peak structural high point and was drilled through an uppermost thin green layer of the St. Peter sandstone to a depth of about 200m [14].

The air injection began on October 2nd, 1982, and stopped on March 21st, 1983. Air with relative humidity less than 5% and temperature close to that of the natural reservoir was injected into the St. Peter sandstone through the I/W well. The bubble development lasted almost 6 months due to the small air flow rate [14].

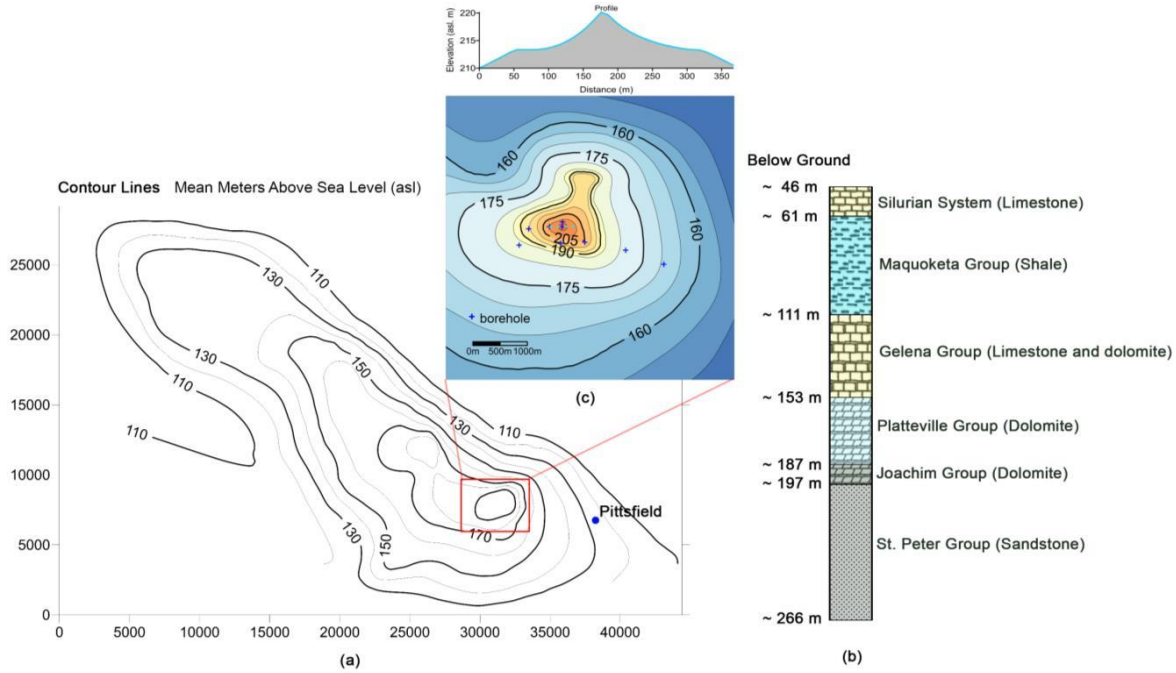

Figure 1. The structure of Pittsfield dome indicated by the uppermost Silurian contours (a); Stratigraphy of Pittsfield dome beneath the Mississippian System (b); and the well-defined closure indicated by the contours of the upper Ordovician Maquoketa shale (c) (Modified from [14])

A conceptual model (Figure 2) is set up based on the Pittsfield aquifer test stratigraphy. The producing length of I/W well is 3 m, which is located in green layer of St. Peter sandstone. The diameter of I/W well is 0.2 m. According to the Pittsfield report [49], the water level is about 108 m beneath the ground surface.

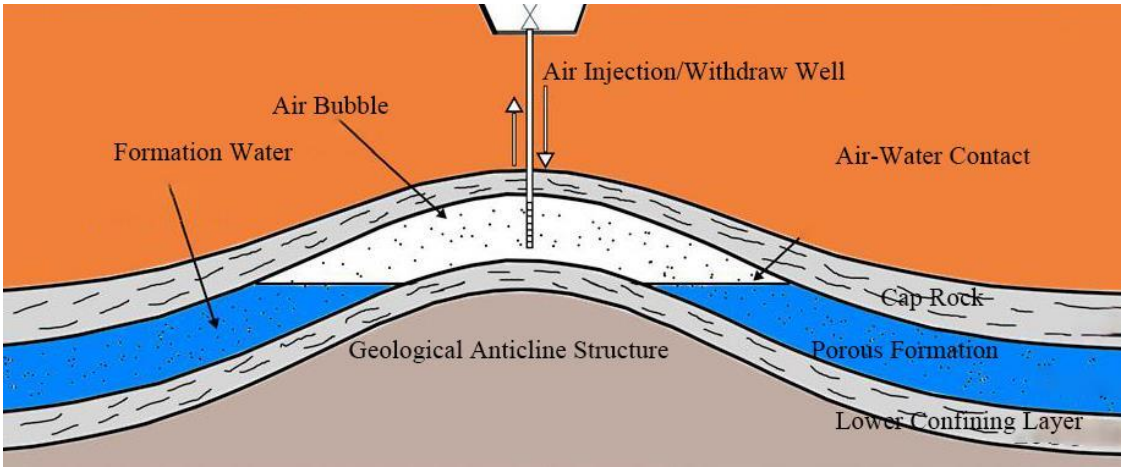

Figure 2. Conceptual model for Pittsfield CAESA model (Modified from [50])

2.2. Numerical Model

2.2.1. Modelling approach

The TOUGH3/EOS3 simulator, developed by Lawrence Berkeley National Laboratory (LBNL) in USA, is used to do the numerical simulations in this study. The TOUGH3 is a general-purpose numerical simulation program for multi-dimensional fluid and heat flows of multiphase, multicomponent fluid mixtures in porous and fractured media. The EOS3 module is developed to describe the system consisting of H_2O-Air-Heat components in a porous medium. The basic mass and energy balance equations solved by TOUGH3/EOS3 can be written in the general form [51]

$$\frac{\mathrm{d}}{dt}\int_{V_n} M^K dV_n = \int_{\Gamma_n} F^K \bullet n d\Gamma_n + \int_{V_n} q^K dV_n \tag{1}$$

where V_n is arbitrary subdomain of integration, Γ_n is the boundary of subdomain, M^k is mass or energy per volume, with k=1, …, NK labeling the mass components (water, air, H_2O), F is mass or heat flux, q is sinks and sources, and n is a normal vector on surface element $d\Gamma_n$, pointing inward into Vn.

The general form of the mass accumulation term is

$$M^K = \phi \sum_{\beta} S_\beta \rho_\beta X_\beta^K \tag{2}$$

where ϕ is porosity, S_β is the saturation of phase β, ρ_β is density of phase β, and X_β^K is the mass fraction of component K present in phase β.

2.2.2. Domain discretization

In the numerical model, the model scale is 3 km×3 km in horizontal and 172 m in vertical. Horizontally, the grids are refined gradually from the boundary to I/W well (Figure 3(a)). The grids size from boundary to wellbore are 100 m×100 m, 50 m×50 m, 10 m×10 m, 5 m×5 m, 2 m×2 m, respectively. The wellbore and its surrounding grids (square area of 4m×4m) are refined as radial grids (Figure 3(b)), with wellbore diameter of 0.2 m in center. Vertically, the thickness of this model is 172 m, including 4 lithologies, which are limestone, impervious dolomite rocks, St. Peter sandstone, and impervious dolomite rocks, respectively. The model is divided into 35 layers and the thickness for each type of lithology are 32 m, 50 m, 70 m and 20 m, respectively (Table 1). The thicknesses of 3 sub-layers of St. Peter sandstone are of 3 m, 6 m, and 61 m, respectively [52].

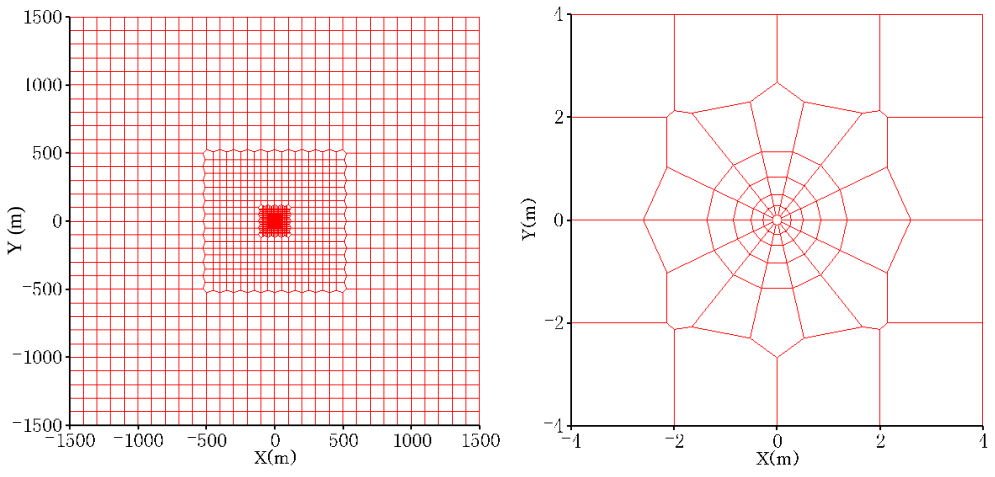

(a) (b)

Figure 3. Domain discretization with grids size from boundary to wellbore of 100m×100m, 50m×50m, 10m×10m, 5m×5m, 2m×2m (a) and wellbore refinement with wellbore diameter of 0.2m in center (b)

Table 1 Vertical layer refinement of Pittsfield model

Lithology	Thickness (m)		Sublayers	Thickness per layer (m)
Limestone (Overburden)	172	32	1	2
			2	15
Dolomite rocks (Cap rock)		50	2	20
			1	6
			2	2
Sandstone (Green layer)		3	3	1
Sandstone (White layer)		6	6	1
Sandstone (Grey layer)		61	6	1
			5	2
			4	5
			1	25
Dolomite rocks (Base rock)		20	2	10

2.2.3. Input parameters

The typical parameters for aquifer and wellbore are shown in Table 2 [21,52]. The initial pressure distribution is in hydrostatic equilibrium with atmospheric pressure at the water level, where the pressure is assumed to be 1.01×10^5 Pa, the discovery pressure at the top of producing screen is 1.0 MPa, and the hydrostatic gradient is 9.8×10^3 Pa/m. In the model, the injection temperature is 20 ℃ with a fixed specified enthalpy, and geothermal gradient is set as 0.03℃/m. The upper boundary is located at 10 m beneath the water level. The pressure and temperature at lateral boundaries are set as hydrostatic pressure and discovery temperature, which means the formation is an open aquifer. The top boundary is set as open boundary and the bottom boundary is closed with no flow and heat transferring.

Table 2. Parameters of aquifer and wellbore in model

Aquifer	**Value**		**Unit**
Grain density	2600		kg/m^3
Heat conductivity	2.16		W/m℃
Grain specific heat	920		J/kg℃
Relative permeability function	Van Genuchten-Mualem model		
Fitting parameter (λ)	0.60		
Residual liquid saturation *(S_{lr})*	0.12		
Saturated liquid saturation *(S_{ls})*	1.00		
Residual gas saturation *(S_{gr})*	0.05		
Capillary pressure function	Van Genuchten function		
Fitting parameter (λ)	0.60		
Residual liquid saturation *(S_{lr})*	0.10		
Minimal capillary pressure *(P_0)*	675.68		Pa
Maximal capillary pressure *(P_{max})*	5.0×10^5		Pa
Saturated liquid saturation *(S_{ls})*	1.00		
Sandstone	**Porosity**	**k_h (m^2)**	**k_v (m^2)**
Green layer	0.17	1.81×10^{-13}	7.60×10^{-14}
White layer	0.16	4.03×10^{-13}	6.62×10^{-13}
Grey layer	0.16	8.70×10^{-13}	7.27×10^{-13}
Wellbore	**Value**		**Unit**

Well Diameter	0.2	m
Well length	200	m
Producing length	3	m

3. Results and discussion

3.1. Feasibility validation of numerical model

Before the carry out of working cycle, a big initial air bubble needs to be developed in the reservoir as a cushion gas for insuring sufficient pressure and avoiding water coning [34]. The mass flow rate of Pittsfield test for initial bubble development is shown in Figure 4. The pre-test analysis indicated that the air flow rate only can be one third of predicted flow rate, so the bubble development lasted about 165 days due to the small air flow rate [14]. The suddenly drop of mass flow rate was caused by the shut-in of plant due to the New Year or Christmas holiday. The discontinuity from the 116th day to the 125th day (about 10 days) occurred during project transfer from the Department of Energy (DOE) to the Electric Power Research Institute (EPRI).

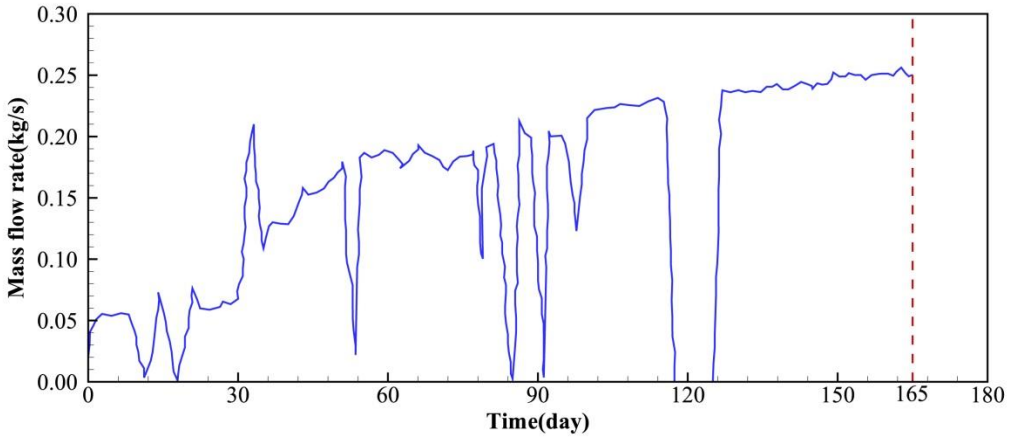

Figure 4. Mass flow rate in I/W well for initial bubble development in 165 days. The suddenly drop was caused by the shut-in of plant

In the numerical model, the simulation result is the pressure at the well bottom, and the pressure drop between wellhead and well bottom can be calculated by [53]

$$\Delta p = \frac{32 \nu \rho u_m L}{D^2} \tag{3}$$

where Δp is pressure drop (Pa); ν is coefficient of viscosity (Ns/m^2); ρ is gas density (kg/m^3); u_m is velocity of gas (m/s); L is well length (m); and D is well diameter (m);.

The comparison of simulation pressure (red line) and monitoring pressure (green squares) at wellhead is shown in Figure 5, which can be seen the reasonable fitting between them. In the first 30 days, the biggest relative error between simulation pressure and monitoring data is 43%. This because at the early stage of the air injection, the air flow inside of wellbore is very complicated due to the quite small mass flow rate, while the monitoring pressure is an average data during each monitoring day. After the first 30 days, the biggest relative error between them is 14%. Because of the transfer of management institution of Pittsfield project, the air injection was stopped about 10 days (from the 116th day to the 125th day), the pressure was dropped from 1.98 MPa to 1.39 MPa.

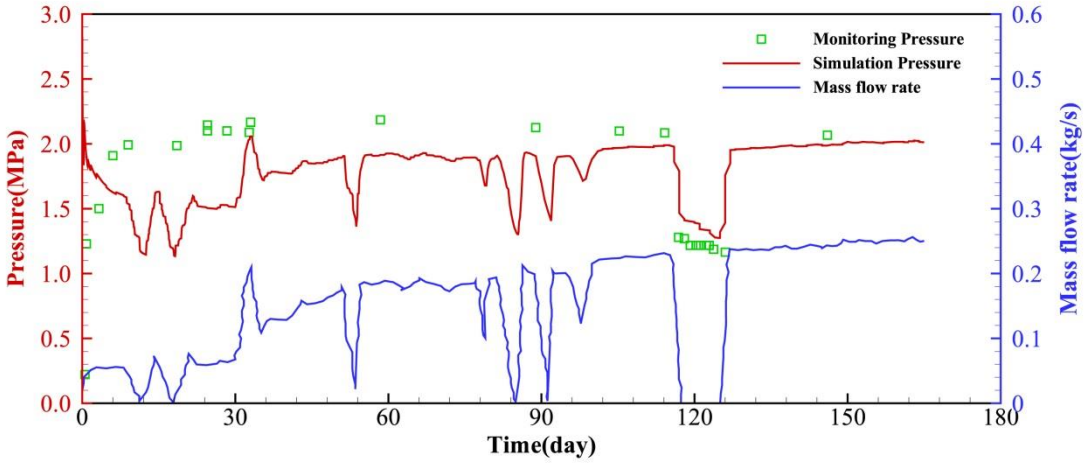

Figure 5. Comparison of simulation pressure (red line) and monitoring pressure at wellhead (green squares). The blue line is mass flow rate

Gas saturation development after air injection of 1 day, 30 days, 90 days and 165 days are shown in Figure 6. The gas saturation of 0.3 is taken as identifier of the plume of effective gas bubble because below this value in model the gas is immobile. It can be seen that as the air injection continues, the compressed air gradually replaces the groundwater away to form an air bubble. The horizontal permeability is bigger than the vertical permeability, so the air plume in horizontal is larger than that in vertical. It can be seen that the plume of air bubble can reach up to about 350 m horizontally. The maximum thickness of air bubble is about 20 m. Generally, the permeability of the cap rock overlying the aquifers is so small that can be considered as impermeable strata. A tiny amount of air transferred to the cap rock in Figure 6 because the cap rock is not absolutely impermeable. This part of air is quite small and can be neglected during the model.

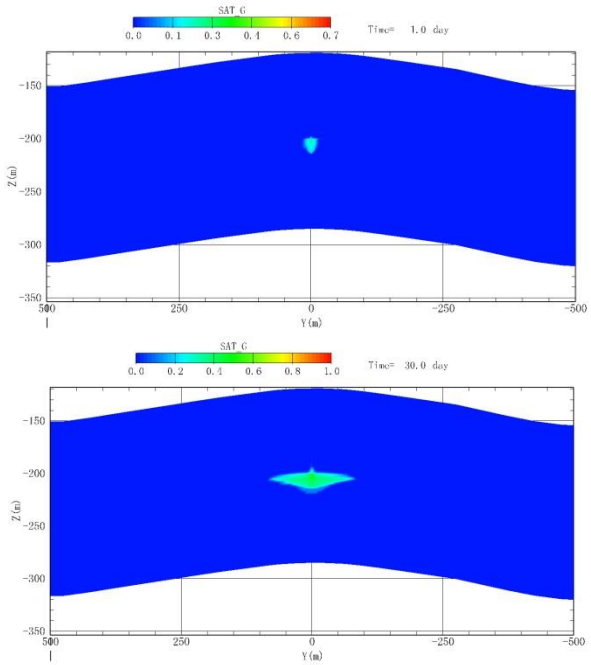

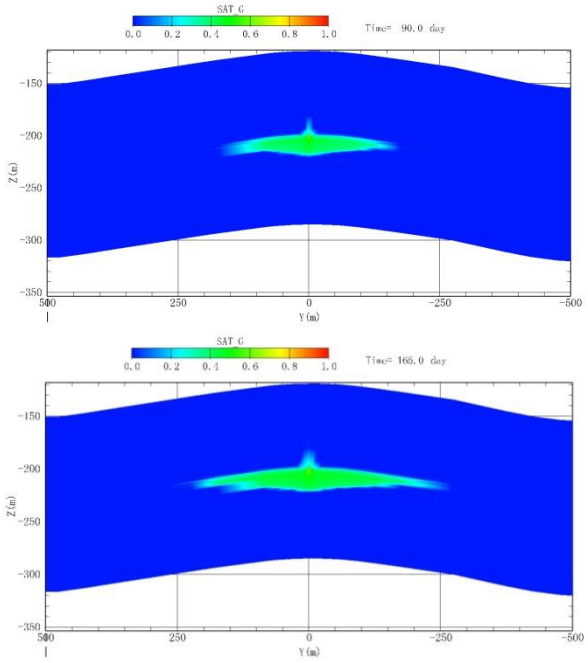

Figure 6. Gas saturation variation at 1 day, 30 days, 90 days and 165 days during the initial bubble development

3.2. Cycle design

3.2.1 Initial bubble development

After the feasibility validation of numerical model, we designed three cycle modes for working cycle, which are daily cycle, weekly cycle, and monthly cycle, respectively. Compressed air with mass flow rate of 2 kg/s is injected into the initial bubble developed aforementioned. The simulation time is one month (28 days). The simulation results indicated that when the production begins, the pressure will decrease to zero immediately. Because according to report from Hydrodynamics group [54], the mass of compressed air in initial bubble should be 10-100 times of mass of compressed air for working cycle. In this study, the mass of initial bubble developed above is about 2.14×10^6 kg (injection time is 165 days and average mass flow rate is about 0.15 kg/s). However, the mass of compressed air for designed working cycle is 2.42×10^6 kg (mass flow rate is 2 kg/s and the injection time is 14 days). It can be calculated that the mass of initial bubble is not enough to support the working cycle. Therefore, a bigger bubble is developed by injection of 5 kg/s compressed air for 165 days. The mass of the bigger bubble is 7.13×10^7 kg, 29.46 times of compressed air mass for working cycle.

Figure 7 shows the bigger bubble development at 1 day, 30 days, 90 days and 165 days. It states that the plume of bubble, where the gas saturation is 0.3, can reach up to 650 m in horizontal, and the biggest thickness of the bubble is about 70 m in vertical. The injection temperature for initial bubble is 20°C with a specified enthalpy and 50℃ for all three types of cycles. In the cycle model, we chose the closed upper boundary, opened lateral boundaries and closed bottom boundary for designed cycles for reducing the boundary effects.

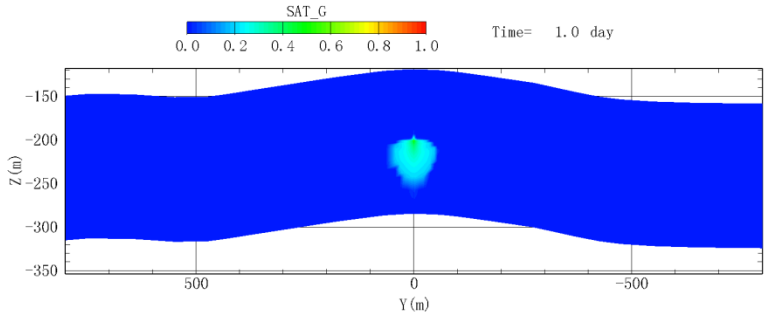

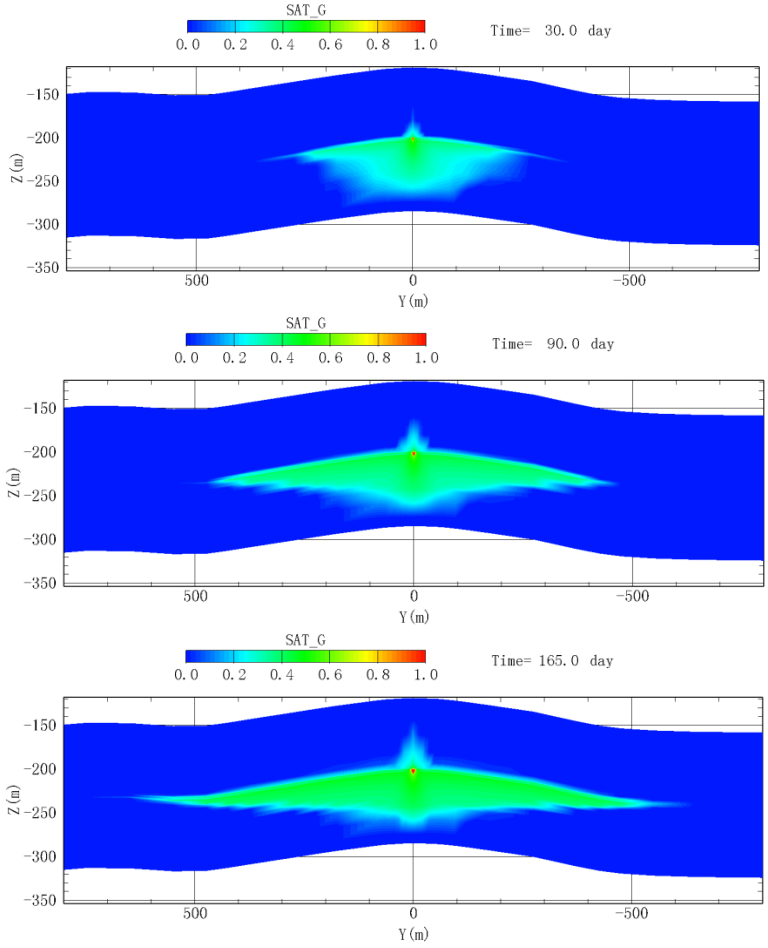

Figure 7 Gas saturation of bigger initial bubble at 1 day, 30 days, 90 days and 165 days with injection rate of 5 kg/s

3.2.2. Pressure performance of three designed cycles

The daily cycle is designed to 12 hours' injection and 12 hours' production, the weekly cycle is 3.5 days' injection and 3.5 days' production, and the monthly cycle is 14 days' injection and 14 days' production (Figure 8). The pressure in aquifers (0.2 m away from I/W well bottom) before working cycle is 4.17 MPa. The pressure drops to 1.93 MPa after the first daily cycle, 1.63 MPa after the first weekly cycle and 1.44 MPa after the monthly cycle. After one month' simulation, the pressure in aquifers (0.2 m away from I/W well bottom) is 1.49 MPa, 1.44 MPa and 1.44 MPa in daily cycle, weekly cycle and monthly cycle, respectively. This is because the compressed air with high pressure transfers to surrounding areas due to the pressure difference, leading to the pressure drop as the cycle continues. As the cycle period of daily cycle is the smallest than weekly cycle and monthly cycle, the energy losses in daily cycle are the smallest, leading to the largest pressure in aquifer of daily cycle after the first cycle finished. As the cycle continues, the rate of energy losses gradually decrease, so the differences of pressure in three cycle modes are small after one month cycle.

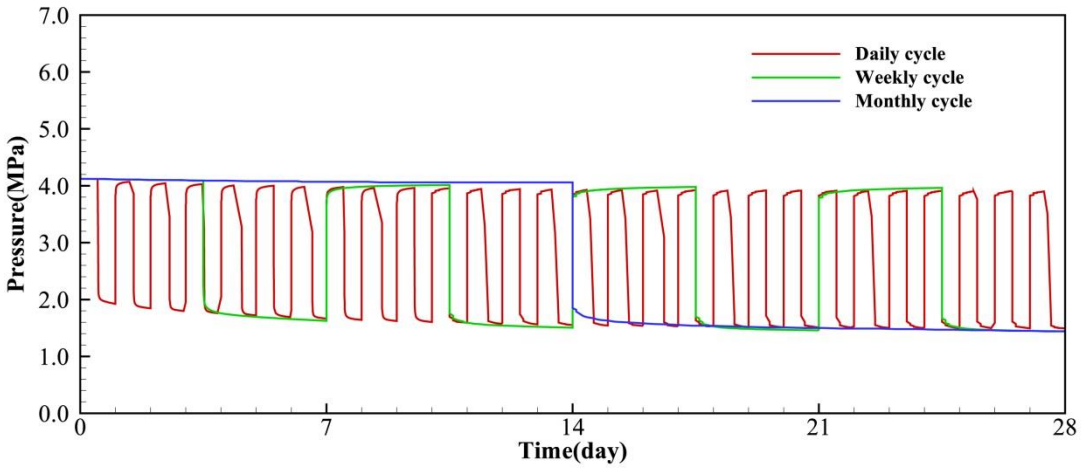

Figure 8. Pressure development in aquifers (0.2 m away from I/W well bottom) in daily cycle (red line), weekly cycle (green line) and monthly cycle (blue line)

3.2.3. Gas saturation of three designed cycles

Figure 9 shows the gas saturation after the first cycle and the last cycle in daily cycle (Figure 9(a) and Figure 9(b)) and weekly cycle (Figure 9(c) and Figure 9(d)), as well as the gas saturation after air injection and production in monthly cycle (Figure 9(e) and Figure 9(f)). After the first cycle (daily cycle and weekly cycle) and air injection (monthly cycle), the depth of bottom edge of gas bubble in daily cycle, weekly cycle and monthly cycle are -263 m, -260 m and -260 m, respectively. The effective volume of the gas bubble will reduce as the cycle continues. This is because the bubble edge gradually breaks into small bubbles and dissipates in the aquifers. After the last cycle, the depth of bottom edge of gas bubble goes up to -252.4m, -252.1 m and -252.2 m, respectively. It is indicated that after one month's cycle, the gas remaining in aquifer has a small difference for the three cycles. That is because the one month's simulation is not long enough to observe the obvious differences among them, and the bubble dissipates slow in aquifer in a month.

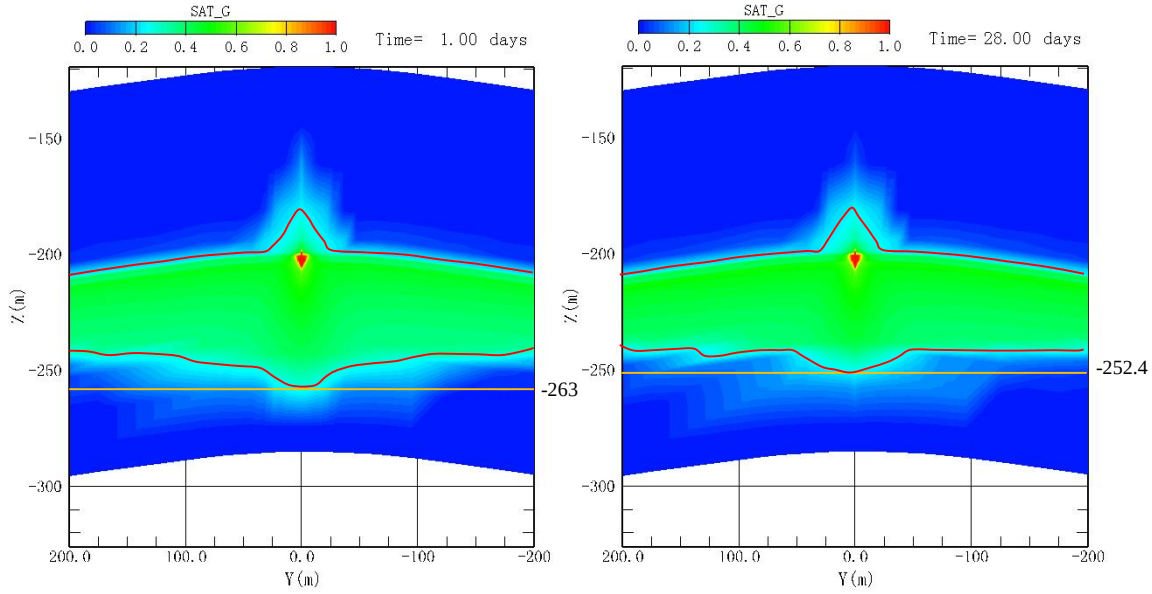

(a) (b)

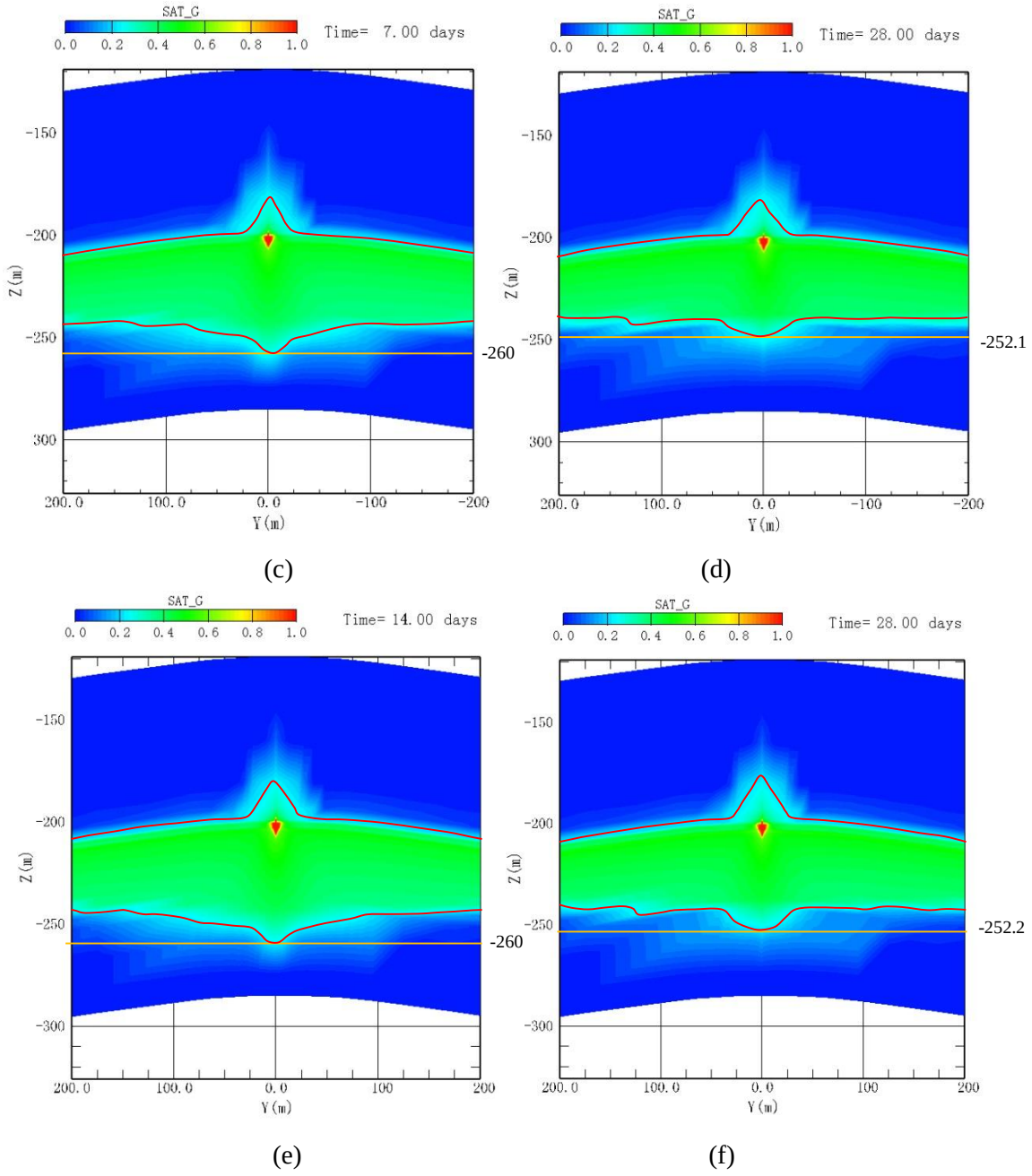

Figure 9. Gas saturation after the first cycle (a) and the last cycle (b) in daily cycle, gas saturation after the first cycle (c) and the last cycle (d) in weekly cycle, and gas saturation after air injection (e) and production (f) in monthly cycle

3.2.4. Temperature variation of three designed cycles

The air temperature injected into the I/W well is 50°C with a fixed enthalpy. Figure 10 shows the temperature variation of three types of cycles. The temperature of initial bubble is 20°C, so when the compressed air with higher temperature injects into the aquifer, the temperature of the bubble increases to 50°C immediately. The temperature decreases when the production carried out. As the cycle continues, the air with higher temperature continuously mixes with low temperature air, leading to gradually increasing of temperature in aquifer. When the cycles were finished, the air temperature in aquifers (0.2 m away from well bottom) are 39°C, 33.6°C and 28.2°C for daily cycle, weekly cycle and monthly cycle, respectively. The increments are 19°C, 13.6°C and 8.2°C, respectively. The cycle times of daily cycle, weekly cycle and monthly cycle in one month are 28 times, 7 times and one time, respectively. It is

indicated that during the same working cycle periods, the more cycle times, the higher air temperature in aquifers after the cycle.

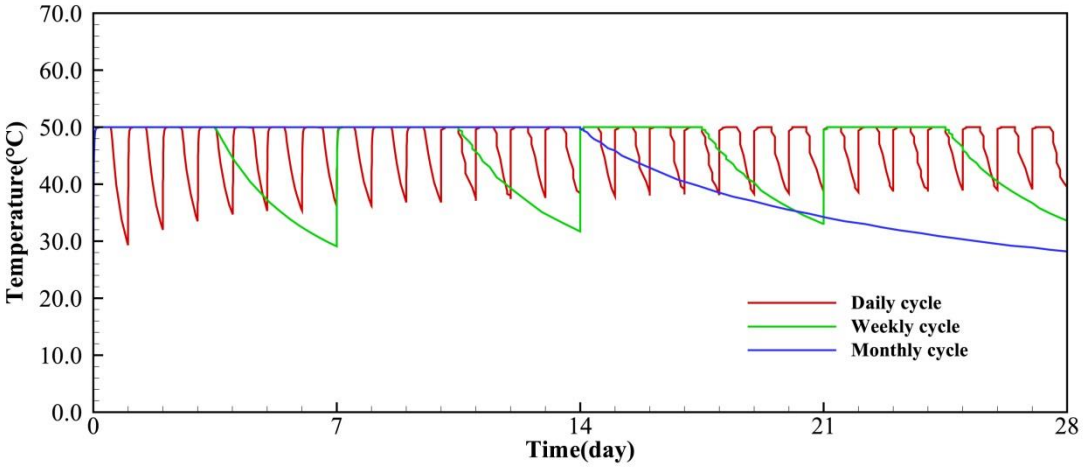

Figure 10. Temperature variations in daily cycle (red line), weekly cycle (green line) and monthly cycle (blue line) in aquifer (0.2 m away from I/W well bottom)

3.2.5. Energy Flow Rate and Energy Recovery Efficiency

The energy flow rates of three cycles at well bottom are shown in Figure 11. A negative value indicates energy production. After one month simulation, the energy flow rate of daily cycle, weekly cycle and monthly cycle are 4.92×10^3 W, 4.69×10^3 W, and 4.46×10^3 W, respectively. It means that after one month cycle, the energy flow rate of daily cycle is slightly larger than the other two. This is because the temperature in daily cycle is the largest in three types of cycle.

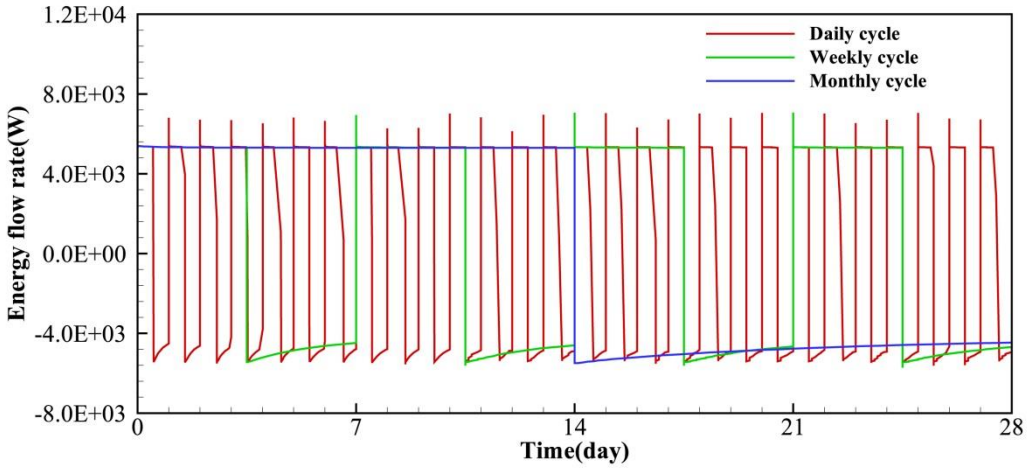

Figure 11. Energy flow rate at I/W well bottom of daily cycle (red line), weekly cycle (green line) and monthly cycle (blue line) during one month cycle

Energy recovery efficiency is defined as the ration of energy produced to energy injected through the wellhead during one cycle or the whole operation cycles:

$$\eta = E_{out}/E_{in} \quad (4)$$

where η is energy recovery efficiency; E_{out} is energy produced through wellhead; E_{in} is energy injected through wellhead.

The energy recovery efficiencies of daily cycle, weekly cycle and monthly cycle at the last cycle can be calculated by Equation 4. The energy flow rate is decreased during the production. In this study, we

chose the average value of energy flow rate during production to obtain the efficiency. For instance, the energy recovery efficiency of daily cycle is calculated as follows:

E_{in}=Energy flow rate×time=5.33×10^3 J/s×12 hours×3600s/hour=2.30×10^8 J

E_{out}=Energy flow rate×time=$(5.4\times10^3+4.92\times10^3)/2\times12$ hours×3600s/hour=2.23×10^8 J

$\eta = E_{out}/E_{in}=2.23\times10^8 /2.30\times10^8=96.96\%$

The energy recovery efficiency for daily cycle, weekly cycle and monthly cycle are 96.96%, 96.27% and 93.15%, respectively. Their energy recovery efficiencies indicate proficient values for practical project of CAESA system. The energy recovery efficiency of daily cycle is slightly higher than weekly cycle and monthly cycle, which stated that more energy is produced in daily cycle due to the higher temperature in aquifer.

4. Conclusions

This study focuses on the application of compressed air energy storage in aquifers with a 3-D numerical model to simulate the multiphase flow and heat transfer in the system. The feasibility of numerical model is investigated. Three types of cycles are designed to investigate their performance, and the energy recovery efficiencies are calculated. The main findings are as follows:

(1) The reasonable fitting between simulation results and monitoring data at wellhead during the bubble development indicates that the model well presents the geological setting of the subsurface system and captures the key heat and multiphase flow processes during air injection.

(2) Adequate pressure in initial bubble is significant to carry out the working cycle in CAESA system. Inadequate pressure will lead to the failure of production, and even bring water coning in CAESA system. After the cycle finished, the depth of bottom edge of gas bubble in daily cycle, weekly cycle and monthly cycle are -252.4m, -252.1m and -252.2m, respectively. It is indicated that after a short time of working cycle, the differences of air consumption in various cycle modes are relatively small. After 28 days' working cycle, the temperature in aquifers (0.2 m away from I/W well bottom) of daily cycle, weekly cycle and monthly cycle increased from 20°C to 39°C, 33.6°C and 28.2°C, respectively. It can be concluded that during the same working cycle periods, the more cycle times, the higher air temperature in aquifers after the cycle.

(3) The energy recovery efficiency for daily cycle, weekly cycle and monthly cycle are 96.96%, 96.27% and 93.15%, respectively. The slight increase of energy recovery efficiencies from daily cycle to monthly cycle indicate that with the same energy storage scales, more energy is produced in daily cycle. A shorter time air injection and production can help improve the performance of a CAESA system which represented by a smaller energy loss to the surrounding formation and remain a large amount of effective compressed air in the CAESA system.

Daily cycle is demonstrated that it is feasible to meet the electric power demand in a short time, but in a practical plant, frequent air injection and production means high operation costs and acceleration of deterioration of facilities such as wellbore tubulars and casing cement through corrosion. In the same cycle period, daily cycle has the most frequent injection and production. It means more energy is needed for combustion the compressed air in turbine after the air was withdrawn, leading to higher operation costs on surface plants. The deterioration of wellbore tubulars and casing cement through corrosion is another important problem to consider for CAES applications. Prominent corrosions include biological, pitting, stress corrosion cracking, fatigue and fretting corrosion, and so on. The promotion of corrosion by air injection might be further exacerbated by high-pressure and high-temperature conditions, especially if significant moisture is present. In theory, long-term cycle will increase the life span of facilities and lead to a more cost-effective operation, which also means reducing nation's dependence on fossil fuels and oils for energy conservation. However, long-term cycle has high requirements to properties of storage reservoirs. Furthermore, the working cycle should be designed according to specific characteristics of renewable energy and the actual power demands of users. In the practical CAESA project, comprehensive consideration should be placed to choose the most cost-efficient CAESA system.

5. Acknowledgements

This research was supported by the fundamental research funds for the Chinese Academy of Geological Sciences, China (Grant No. DD20201165, JYYWF20180301, JKY202004, YWF201903, 2019YFB1504102 and DD20190707), and Dr. Lawrence Ho Research and Development Fund partly support the first author conducting this research at Edinburgh Napier University, UK.

References

1. EPRI (Electric Power Research Institute). Electric Energy Storage Technology Options, A Primer on Applications, Costs & Benefits, EPRI, Palo Alto, CA, 2010.
2. Zhiqiang Jiang, Changming Ji, Hui Qin, Zhongkai Feng. Multi-stage progressive optimality algorithm and its application in energy storage operation chart optimization of cascade reservoirs. Energy 2018;148: 309-323.
3. Zhiqiang Jiang, Rongbo Li, Anqiang Li, Changming Ji. Runoff forecast uncertainty considered load adjustment model of cascade hydropower stations and its application. Energy 2018;158: 693-708.
4. Oldenburg C M, Pan L. Porous Media Compressed-Air Energy Storage (PM-CAES): Theory and Simulation of the Coupled Wellbore–Reservoir System. Transport in Porous Media 2013; 97(2):201-221.
5. Luo Xing, Wang Jihong, Dooner Mark, Clarke Jonathan. Overview of current development in electrical energy storage technologies and the application potential in power system operation. Applied Energy 2015;137: 511-536.
6. Budt M , Wolf D , Span R , Yan J. A review on compressed air energy storage: Basic principles, past milestones and recent developments. Applied Energy, 2016; 170: 250-268.
7. Arman Aghahosseini, Christian Breyer. Assessment of geological resource potential for compressed air energy storage in global electricity supply. Energy Conversion and Management. 2018; 169: 161-173.
8. Beckwith. Review of environmental studies and issues on compressed air energy storage. Pacific Northwest Laboratory. 1983, PNL-4460.
9. Shang Chen, Ahmad Arabkoohsar Tong Zhu, Mads Pagh Nielsen. Development of a micro-compressed air energy storage system model based on experiments. Energy 2020; 197: 117152.
10. Ghady Dib, Philippe Haberschill, Romuald Rulliere Quentin Perroit, Simon Davies, Remi Revellin. Thermodynamic simulation of a micro advanced adiabatic compressed air energy storage for building application. Applied Energy 2020; 260: 114248.
11. Mandhapati Raju, Siddhartha Kumar Khaitan. Modeling and simulation of compressed air storage in caverns: A case study of the Huntorf plant. Applied Energy 2012: 474-481.
12. CROTOGINO F, MOHMEYER K-U, SCHARF R. Huntorf CAES: More than 20 years of successful operation//Proceedings of the AKE.
13. SUCCAR S, WILLIAMS R H, Compressed air energy storage: theory, resources, and applications for wind power, NRC000040: PEI, 2008.
14. R.D. Allen, T.J. Doherty, L.D. Kannberg, Summary of selected compressed air energy storage studies, Pacific Northwest Laboratory. 1985. PNL-5091.
15. Braester C, Bear J. Some hydrodynamic aspects of compressed-air energy storage in aquifers. Journal of Hydrology 1984; 73(3-4): 201-225.
16. Kushnir R, Ullmann A, Dayan A. Compressed Air Flow within Aquifer Reservoirs of CAES Plants. Transport in Porous Media 2010; 81(2):219-240.
17. Y Huang, HS Chen, XJ Zhang, P Keatley, MJ Huang, I Vorushylo, et al. Techno-economic modelling of large scale compressed air energy storage systems. Energy Procedia 2017; 105: 4034-4039.
18. Mehdi Ebrahimi, Rupp Carriveau, David S.-K. Ting, Andrew McGills. Conventional and advanced exergy analysis of a grid connected underwater compressed air energy storage facility. Applied Energy 2019; 242: 1198-1208.
19. Guo C, Pan L, Zhang K, Oldenburg C, Li C, Li Y. Comparison of compressed air energy storage process in aquifers and caverns based on the Huntorf CAES plant. Applied Energy 2016; 181:342-356.
20. R. D. Allen, T. J. Doherty, R. L. Erikson, L. E. Wiles. Factors affecting storage of compressed air in porous rock reservoirs. Pacific Northwest Laboratory 1983. PNL-4707.
21. R.D. Allen, L.D. Kannberg, T.J. Doherty. Aquifer field test for compressed air energy storage. In proceedings of the 16th intersociety energy conversion engineering conference. 1981: 978-983.
22. Istvan. J.A. Compressed-Air energy storage field test using the aquifer at Pittsfield, Illinois. 1991. GS-6671.

23. Smith G C, Wiles L E. Analysis of underground porous reservoirs for compressed air energy storage; proceedings of the Compressed Air Energy Storage Symposium Porceedings, Springfield, Virginia, F, 1979. National Technical Information Service.
24. Jarvis A-S. Feasibility study of porous media compressed air energy storage in South Carolina, United States of America, Clemson University, 2015.
25. Pei P, Scott F. Korom, Ling K, He J, Andres G. Thermodynamic impact of aquifer permeability on the performance of a compressed air energy storage plant. Energy Conversion and Management 2015; 97:340-350.
26. Li Y, Pan L, Zhang K, Hu L, Wang J, Guo C. Numerical modeling study of a man-made low-permeability barrier for the compressed air energy storage in high-permeability aquifer. Applied Energy. 2017; 208: 820-833.
27. Guo C, Zhang K , Li C , Wang X. Modelling studies for influence factors of gas bubble in compressed air energy storage in aquifers. Energy 2016; 107: 48-59.
28. Wang B, Bauer S. Pressure response of large-scale compressed air energy storage in porous formations. Energy Procedia 2017; 125 (1): 588-595.
29. Wiles L E, Oster C A. Fluid flow and thermal analysis for CAES in porous rock reservoirs; proceedings of the In Proceedings of the 1978 Mechanical and Magnetic Energy Storage Constractors' Review Meeting, Springfield, Virginia, F, 1978. National Technical Information Service.
30. Oldenburg, Curtis M, Lehua Pan. Utilization of CO_2 as cushion gas for porous media compressed air energy storage. Greenhouse Gases Science & Technology 2013; 3(2):124-135.
31. Li Y, Zhang K, Hu L, Wang J. Thermodynamic analysis of heat transfer in a wellbore combining compressed air energy storage. Environmental Earth Sciences. 2017; 76(6): 247.
32. Lukasa Bartela. A hybrid energy storage system using compressed air and hydrogen as the energy carrier. Energy 2020; 196: 117088.
33. Eide Hammann, Reinhard Mdlener, Christoph Hilgers. Economic feasibility of a compressed air energy storage system under market uncertainty: a real options approach. Energy Procedia 2017; 105: 3798-3805.
34. Wiles L E, Mccann R A. Water coning in porous media reservoirs for compressed air energy storage. Nasa Sti/recon Technical Report N, 1981, 82.
35. Kushnir R, Ullmann A, Dayan A. Thermodynamic and hydrodynamic response of compressed air energy storage reservoirs: a review. Reviews in Chemical Engineering 2012: 123-148.
36. Allen R D, Doherty T J, Erikson R L. PNL-4707: Pacific Northwest Lab, Richland, WA (USA), 1983.
37. Qian Zhou, Dongmei Du, Chang Lu, Qing He, Wenyi Liu. A review of thermal energy storage in compressed air energy storage system. Energy 2019; 188: 115993.
38. Wang S, Zhang X, Yang L, Zhou Y, Wang J. Experimental study of compressed air energy storage system with thermal energy storage. Energy, 2016; 103: 182-191.
39. Guo C, Zhang K, Pan L, Cai Z, Li C, Li Y. Numerical investigation of a joint approach to thermal energy storage and compressed air energy storage in aquifers. Applied Energy 2017; 203: 948-958.
40. Houssainy S, Janbozorgi M, Ip P, Kavehpour P. Thermodynamic analysis of a high temperature hybrid compressed air energy storage (HTH-CAES) system. Renewable Energy. 2018; 115: 1043-1054.
41. Min J Kim, Tong S Kim. Feasibility study on the influence of steam injection in the compressed air energy storage system. Energy. 2017; 141: 239-249.
42. Yi L, Keni Z, Litang H, Wang J. Numerical Investigation of the Influences of Wellbore Flow on Compressed Air Energy Storage in Aquifers. Geofluids. 2017: 1-14.
43. Erwan Adi Saputro, Mohammed M. Farid. A novel approach of heat recovery system in compressed air energy storage (CAES). Energy Conversion and Management 2018; 178: 217-225.
44. He Q, Li G, Lu C, Du D, Liu W. A compressed air energy storage system with variable pressure ratio and its operation control. Energy. 2019; 169: 881-894.
45. L.E. Wiles, R.A. McCann. Reservoir characterization and final pre-test analysis in support of the compressed air energy storage Pittsfield aquifer field test in Pike County, Illinois. Pacific Northwest Laboratory. 1983. PNL-4743.
46. Istvan J, Crow C, Pereira J. Compressed Air Energy Storage (CAES) in an aquifer-a case history; proceedings of the SPE annual technical conference and exhibition, F, 1983. Society of Petroleum Engineers.
47. David K. Davies. Pre-test geological and geochemical evaluation of the caprock, St. Peter sandstone and formation fluids Yakley field, Pike County, Illinois. Pacific Northwest Laboratory. 1983. PNL-4564.

48. R.L. Erikson. Thermophysical behavior of St. Peter sandstone: Application to compressed air energy storage in an aquifer. Pacific Northwest Laboratory. 1983. PNL-4812.
49. D.D. Hostetler, S.W. Childs, S.J. Phillips. Subsurface monitoring of reservoir pressure, temperature, relative humidity, and water content at the CAES field experiment, Pittsfield, Illinois: System design. 1983. PNL-4687.
50. Wang B, Sebastian Bauer. Compressed air energy storage in porous formations: a feasibility and deliverability study. Petroleum Geoscience 2017; 23: 306-314.
51. Jung Y, Pau S, Stefan Finsterle, Christine Doughty. TOUGH3 User's Guide. Lawrence Berkeley National Laboratory. 2018.
52. Bui, H. V., Herzog R.A., Jacewicz D.M., et al. Compressed-air energy storage: Pittsfield aquifer field test. Electric Power Research Institute. 1990. EPRI-GS-6688.
53. Frank. P. Incropera, David P. Dewitt, Theodore L. Bergman, Adrienne S. Lavine. Fundamentals of heat and mass transfer. 2007.
54. Final project report Dallas center MT. Simon structure CAES system performance analysis. DesMoines, Iowa: The Hydrodynamics Group, 2011.